Perspective on Trions and Excitons in Two-Dimensional Atomically Thin Materials

Yaroslav V. Zhumagulov[1] and Vasili Perebeinos[2]*
[1] *Institute for Theoretical Physics, University of Regensburg, 93040 Regensburg, Germany and*
[2] *Department of Electrical Engineering, University at Buffalo, The State University of New York, Buffalo, New York 14260, USA*
(Dated: December 6, 2024)

Charged excitons or trions are essential for optical spectra in low-dimensional doped monolayers of transitional metal dichalcogenides. This Perspective aims to provide an overview of theoretical approaches that can be employed to predict optical spectra, including many-body interactions leading to tightly bound excitons and trions. The approaches include solutions of the Bethe-Salpeter Equation for excitons and the Tamm-Dancoff equation for trions. The resulting energy spectra and two-body exciton wavefunctions and three-body trion wavefunctions allow calculations of transition matrix elements for optical spectra in transition-metal dichalcogenide monolayers as a function of doping, temperature, dielectric environment, and in the presence of an optical cavity. The external control by doping and dielectric environment allows tuning of the fine structure of the trion and exciton energies, leading to the anticrossing of the bright and dark states, enabling expanded or superior optical device functionality.

I. INTRODUCTION

Transition-metal dichalcogenides (TMDCs) have become the subject of intense research interest in recent years, particularly in optoelectronics. One of the key properties of TMDCs that has garnered attention is the formation of trions, charge-bound complexes that consist of a negatively charged exciton. This Perspective provides a comprehensive overview of the current knowledge on trions and excitons in TMDCs, including their formation mechanisms, optical properties, and potential applications. Our comprehensive overview of the optical properties of trions and excitons in transition-metal dichalcogenides includes bright and dark excitonic states, and the factors that influence photoluminescence excitation spectra and their efficiency and brightness.

The two-dimensional (2D) geometry of TMDCs significantly enhances the Coulomb interaction, leading to the formation of excitons, strongly bound electron-hole pairs with binding energy[1–6] much higher than that of bulk semiconductors[7–9]. 2D confinement also facilitates the formation of other many-body states, including charged three-particle trions[10–19] and charge-neutral four-particle biexcitons[20–26] with high binding energies.

A complex band structure featuring two direct band gaps at the K and $K' = -K$ points of the Brillouin zone, combined with the spin-valley locking effect[27–30], enables the realization of diverse trionic and excitonic states in the TMDC monolayer[31–45]. Typically, trions are classified by spin and valley quantum numbers, and they can be dark or bright depending on the combination of the quantum numbers. The trionic fine structure determines the optical absorption edge and the photoluminescence spectra. In particular, the photolumenescence spectra and their temperature behavior[40,46–49] strongly depend on whether the ground trion state is optically bright or dark, which in turn depends on multiple factors such as spin-orbit coupling, direct and exchange Coulomb interactions, and carrier doping level[32,36,38,39,50]. For example, Ref.[51] investigates the intervalley electron-hole exchange interaction and impurity-assisted recombination of indirect excitons in WS_2 and WSe_2 monolayers. This study provides a comprehensive analysis of the unique interplay between the spin and valley degrees of freedom observed in excitonic states within tungsten-based dichalcogenide monolayers. Similarly, Ref.[52] explores the interaction-driven transport dynamics of dark excitons in WS_2, highlighting their potential for long-range information transfer in quantum information technologies. It demonstrates that excitons can propagate over several micrometers, benefiting from strong repulsive interactions and phonon-mediated optical readout, offering a significant advancement in using excitonic quantum fluids for data manipulation and storage. Most recently, phonon-assisted exciton Auger non-radiative decay in doped TMDCs was considered in[53]. The goal of this Perspective is to review the available computational approaches to explain and predict a wide range of experimental observations, including linear absorption and photoluminescence, non-linear spectroscopy, and the response of excitons and trions to external electric fields.

II. THEORETICAL APPROACHES FOR EXCITONS AND TRIONS

A. Bethe-Salpeter Equation for two-particle exciton

Before we discuss the calculation of three-particle trion states in transition metal dichalcogenides (TMDCs), it is important to briefly introduce the methods for calculating excitonic states. Various approaches, such as the variational method[35,55–59] and the Bethe-Salpeter equation (BSE)[60–66], can be used, each with its strengths and limitations. The exciton calculation involves solving the Schrödinger equation for the electron-hole pair, focusing on the interaction potential, which is crucial

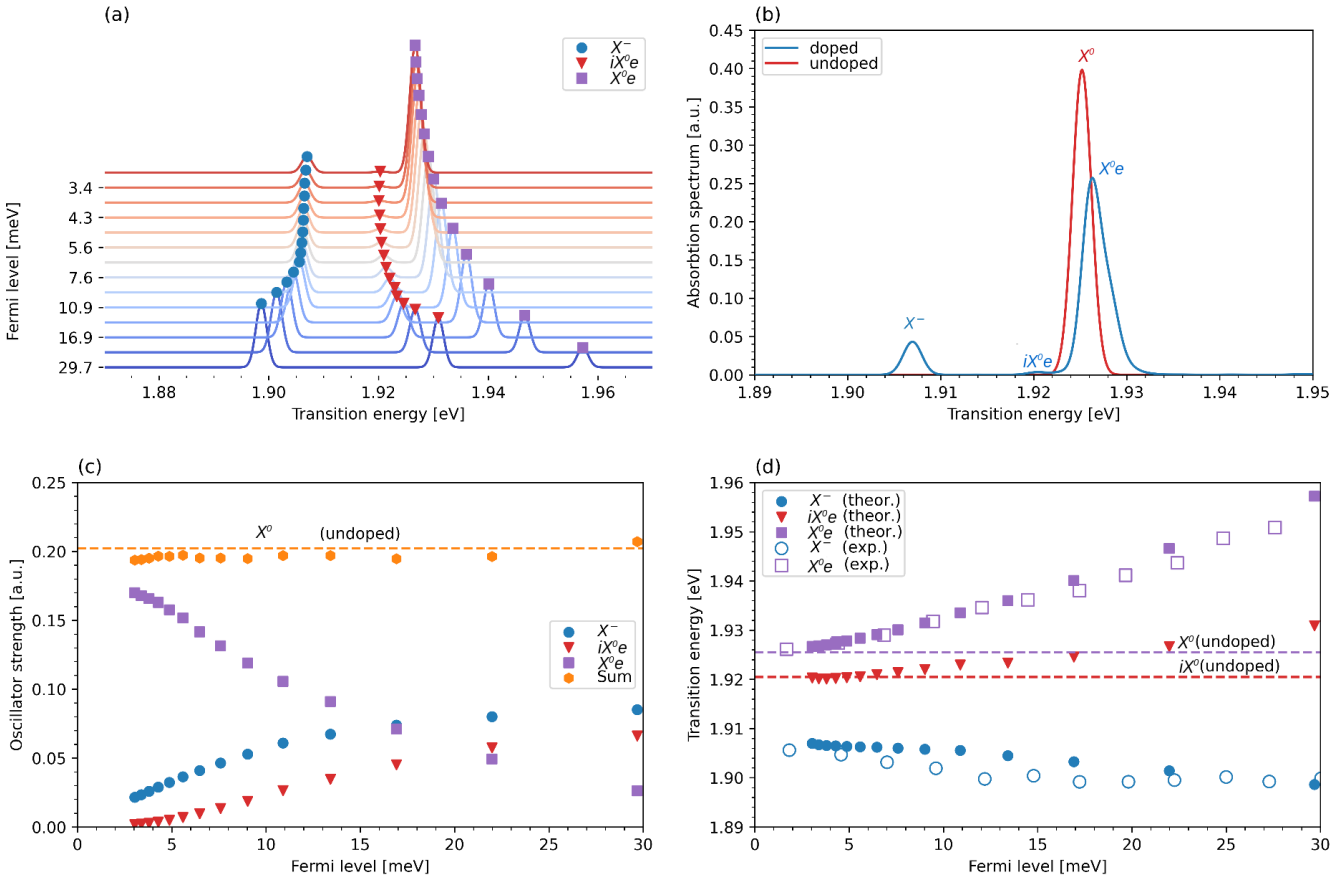

FIG. 1. (a) Absorption spectrum of MoS_2 monolayer calculated for different values of the Fermi levels E_F (shown on the left), the lines are offset vertically for clarity. The three peaks X^-, iX^0e and X^0e correspond to trion, indirect exciton, and exciton [54]. (b) Absorption spectra of the undoped (red) and doped (blue) monolayers at the Fermi level $E_F = 3.04$ meV. (c) The oscillator strength of the spectral peaks and the total oscillator strength (the sum of the three peaks) are functions of the Fermi level. The dashed line gives the oscillator strength of the X exciton peak of the undoped system. (d) The energy position of the peaks as a function of the Fermi level, experimental data[10] for the two peaks energies X^- and X^0e are shown for comparison. The dashed lines show the intervalley iX^0 and intravalley X^0 exciton energies according to the BSE solution in the undoped system. Adapted from[54].

for determining the exciton's binding energy and other properties; for TMDCs monolayers a common choice is the Rytova-Keldysh potential[67–70], widely applied in two-dimensional insulating systems. The variational approach uses the effective mass approximation, simplifying the exciton Hamiltonian but is less precise in capturing certain exciton behaviors. In contrast, the BSE employs many-body perturbation theory, providing a more accurate description of exciton properties, including their optical spectra and binding energies.

BSE is a modern key tool for modeling excitons in materials, as it accounts for the exchange and direct interactions between electron-hole pairs beyond the independent-particle approximation. Calculation of exciton states is performed by direct diagonalization of the two-body Hamiltonian obtained by spanning the many-body model into electron-hole pair states $|cv\rangle = a_c^\dagger a_v |0\rangle$, where c and v are single-particle electron and hole states, respectively. The ground state $|0\rangle$ has a filled valence band and an empty conduction band. Thus BSE Hamiltonian reads as follows:

$$\begin{aligned} H =& H_0 + H_{cv}, \\ H_0 =& (\varepsilon_c - \varepsilon_v)\delta_c^{c'}\delta_v^{v'}, \\ H_{cv} =& -(W_{v'c}^{c'} - V_{v'c}^{c'v}) \end{aligned} \tag{1}$$

where $\varepsilon_{c,v}$ are single-particle energies, W and V are the screened and bare Coulomb potentials components, responsible for direct and exchange interaction, respectively. The numerical implementation of the general Eq. (1) can be performed in the single particle basis set obtained from *ab initio* density functional theory[36], tight-binding model[54], or Dirac model Hamiltonian[40].

In this Perspective, we will focus on the massive $k \cdot p$ Dirac model[71], which can efficiently describe the low-

	a [Å]	d [Å]	ε_{bulk}	Δ_0 [eV]	m	λ_c [meV]	λ_v [meV]
MoS_2	3.185	6.12	16.3	2.087	0.520	-1.41	74.60
$MoSe_2$	3.319	6.54	17.9	1.817	0.608	-10.45	93.25
WS_2	3.180	6.14	14.6	2.250	0.351	15.72	213.46
WSe_2	3.319	6.52	16.0	1.979	0.379	19.85	233.07

TABLE I. Model parameters for TMDC monolayers: lattice constant a, effective mass m, and spin-orbit couplings $\lambda_{c,v}$ are taken from Ref.[74]. The layer thickness d and bulk dielectric constant ε_{bulk} are from Ref.[78], and bandgap Δ_0 is from Ref.[73].

energy single-particle states of TMDCs monolayers:

$$H_D = v_F \hat{s}_0 \otimes \left(\tau k_x \hat{\sigma}_x + k_y \hat{\sigma}_y\right) + \frac{\Delta}{2}\hat{s}_0 \otimes \hat{\sigma}_z + \frac{1}{2}\tau \hat{s}_z \otimes \left[\lambda_c(\hat{\sigma}_0 + \hat{\sigma}_z) + \lambda_v(\hat{\sigma}_0 - \hat{\sigma}_z)\right], \quad (2)$$

where $\hat{\sigma}_i$ are the Pauli matrices in the band subspace, $\hat{s}_z$ is the Pauli matrix in the spin subspace, $\hat{\sigma}_0$ and $\hat{s}_0$ are unity matrices, $\tau = \pm 1$ is the valley index for K and $K' = -K$, v_F is the effective Fermi velocity, and Δ is the bandgap. The last contribution to Eq. (2) describes the Zeeman spin-orbit coupling with constants $\lambda_{c,v}$. The parameters Δ and $\lambda_{c,v}$ are obtained by fitting the *ab initio* band structure calculations using the DFT / GW approaches[72–74]. The gap Δ depends on the encapsulating materials and needs a correction, for example, using the scissor operator approach when quantitatively accurate results are required[75]. It is known that the dielectric environment does not change the effective mass of the single-particle states[76]. The role of dielectric environment on exciton binding energies has been demonstrated in heterostructures in Ref.[77]. For complete reproducibility of our results, all tabulated parameters parameterizing the massive Dirac Hamiltonian and screened Coulomb potential are presented in Table I.

In addition to the massive Dirac model, for simplicity, in this Perspective we will focus on the latter V_{cd}^{ab} given by $V_{cd}^{ab} = V(\mathbf{k}_a - \mathbf{k}_c)\langle u_c|u_a\rangle\langle u_d|u_b\rangle$ with $\langle u_c|u_a\rangle$ the overlap of the Bloch states of a single particle and $V(q) = 2\pi e^2/q$. For the intravalley screened potential, we follow Ref.[55] and substitute $V(q)$ in this expression by the Rytova-Keldysh $W(q)$ potential[67–70]

$$W(q) = V(q)\begin{cases}\varepsilon_{env}^{-1}(1 + r_0 q)^{-1} & q - \text{intravalley} \\ \varepsilon_{bulk}^{-1} & q - \text{interavalley}\end{cases}, \quad (3)$$

where "intravalley" stands for the states within the same valley, and "intervalley" is for states in different valleys. For the encapsulating material, the effective dielectric constant $\varepsilon_{env} = (\varepsilon_2 + \varepsilon_1)/2$ is the average of dielectric constants on both sides of the monolayer, and the screening length is $r_0 = \varepsilon_{bulk} d/(2\varepsilon_{env})$ with d being the width of the monolayer[55,75]. Notice that the finite-intervalley dielectric screening induces the intervalley interaction between pairs of trion states. It was not observed in previous works where only the Keldysh potential was used[40,54]. The more general form of the latter V_{cd}^{ab} for ab initio parametrization can be found in[80].

To determine exciton wavefunctions, energies and absorption spectrum, the following eigenvalue problem must be solved:

$$\sum_{c'v'} H_{cv}^{c'v'} A_{c'v'}^X = E_X A_{cv}^X, \quad (4)$$

where E_X represents the energy of the X-th exciton, and $A_{c'v'}^X$ is its corresponding wavefunction. The transition matrix elements are calculated using the expression:

$$\langle X|\hat{\mathbf{P}}|0\rangle = \sum_{cv} p_{cv}^{\alpha} A_{cv}^X, \quad (5)$$

where $p_{cv}^{\alpha} = \langle c|p^{\alpha}|v\rangle$ denotes the transition matrix element in the α direction between the conduction state c and the valence state v. Consequently, the linear exciton absorption spectrum is given by the sum of transition rates between all exciton states and the ground state $|0\rangle$, expressed as:

$$L_X(E) \propto \sum_X \left|\langle X|\hat{\mathbf{P}}|0\rangle\right|^2 \delta\left(E - E_X\right), \quad (6)$$

where the summation is performed over all exciton states X. Thus, we have completed the explanation of the approach for calculating exciton states in TMDCs monolayers in this Perspective, by preparing the foundation for further expansion of the approach by adding an electron (hole) to explain the approach for calculating trion states in these materials.

B. Tamm-Dancoff Equation for three-particle trion

There are two main theoretical approaches for studying trion states in monolayers of transition metal dichalcogenides: the few-particle trion approach[35,36,38,39,55–59,80–91] and the many-body Fermi-polaron approach. First proposed for the theoretical analysis of inverse radio frequency spectroscopy experiments in two-component Fermi gases[92–95], the Fermi-polaron approach was extended to study charged exciton complexes - trions in monolayers of TMDCs[33,88,96–103]. The Fermi-polaron approach is partially phenomenological, since the exciton-electron interaction often takes a phenomenological form. Microscopic calculation of exciton-electron interaction involves solving the few-body trion problem [104,105]. Despite differences between approaches, few-body trion, and Fermi-polaron, both yield equivalent results in the linear response regime for low levels of electron doping in the system[106]. At high carrier densities, the formation of tetrons consisting of four particles was proposed[107] when a trion becomes bound to

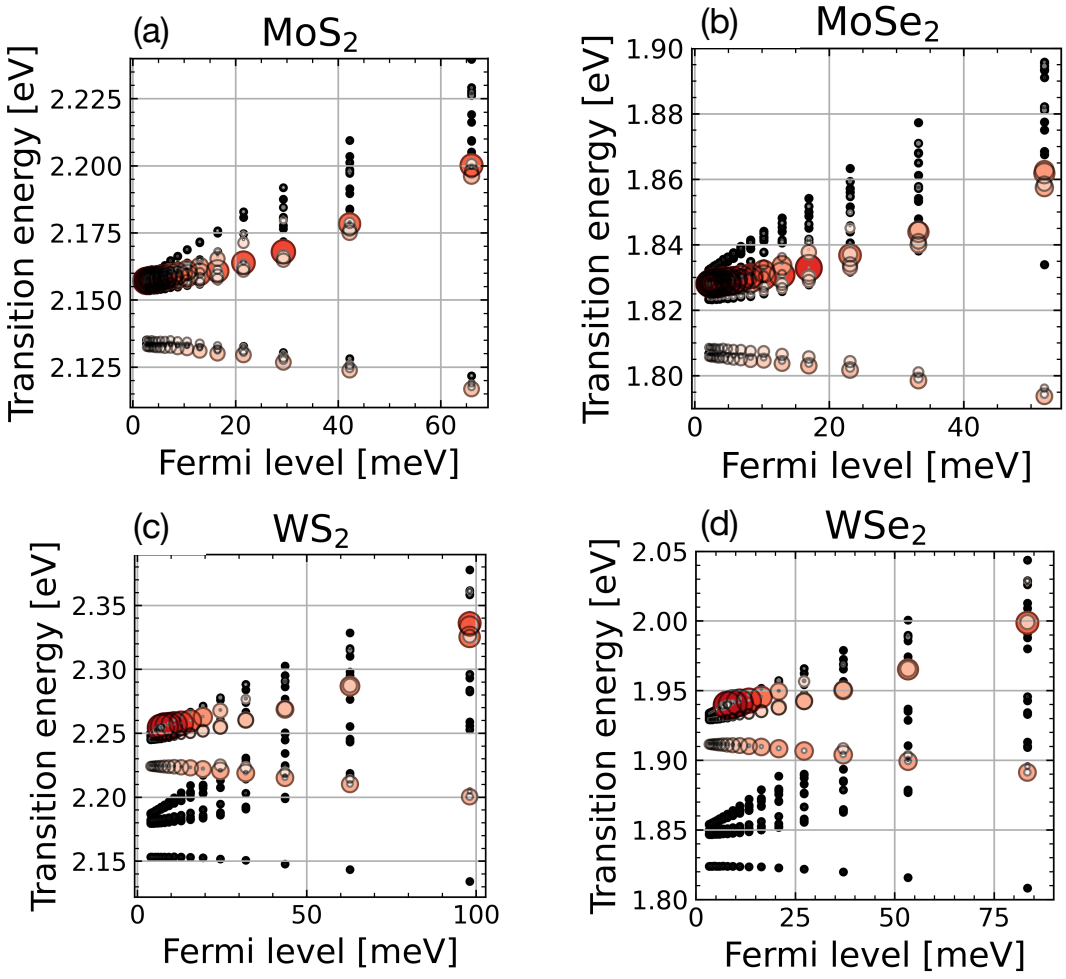

FIG. 2. Energy diagram of the transition energies of the three-particle states calculated in freestanding ($\varepsilon_{env} = 1$) monolayers of MoS_2 (a), $MoSe_2$ (b), WS_2 (c), and WSe_2 (d) as a function of the Fermi level. Circle centers denote the optical transition energies of trions. The color and width indicate their oscillator strengths (red) for bright states and (black) for dark ones. "Trion" and "exciton" denote trion and exciton states, depending on whether the second electron in the three-particle wavefunction is bound or not. Adapted from[79].

a Fermi hole in the conduction band. In this Perspective, we will mainly consider the few-body trion approach.

The most common method for calculating trion states is the Tamm-Dancoff three-particle Equation. First formulated in Ref.[80], it has been widely applied to a variety of systems, such as carbon nanotubes[80], carbon nanoribonns[84], black phosphorus monolayers[83], and TMDCs[36,38,39,81,82,84,85,90]. This method can work beyond the variational approach, limited by the effective mass approximation; therefore, a first-principles parametrization of the Tamm-Dancoff equation is possible[80].

The Tamm-Dancoff three-particle Equation is based on the extension of the Bethe-Salpeter Equation with an additional set of diagrams responsible for the third, electron or a hole particle. The calculation of trion states is performed by a direct diagonalization of the three-body Hamiltonian obtained by spanning the many-body model into states with two electrons and a hole (we consider negatively charged trions) $|c_1 c_2 v\rangle = a^\dagger_{c_1} a^\dagger_{c_2} a_v |0\rangle$, where $c_{1,2}$ and v are single-particle electron and hole states, respectively. The ground state $|0\rangle$ has a filled valence band and an empty conduction band. The Hamiltonian reads as follows:

$$\begin{aligned} H =& H_0 + H_{cc} + H_{cv}, \\ H_0 =& (\varepsilon_{c_1} + \varepsilon_{c_2} - \varepsilon_v)\delta^{c_1'}_{c_1}\delta^{c_2'}_{c_2}\delta^{v'}_{v}, \\ H_{cc} =& (W^{c_1' c_2'}_{c_1 c_2} - W^{c_2' c_1'}_{c_1 c_2})\delta^{v'}_{v}, \\ H_{cv} =& -(W^{v c_1'}_{v' c_1} - V^{c_1' v}_{v' c_1})\delta^{c_2'}_{c_2} - (W^{v c_2'}_{v' c_2} - V^{c_2' v}_{v' c_2})\delta^{c_1'}_{c_1} \\ &+ (W^{v c_2'}_{v' c_1} - V^{c_2' v}_{v' c_1})\delta^{c_1'}_{c_2} + (W^{v c_1'}_{v' c_2} - V^{c_1' v}_{v' c_2})\delta^{c_2'}_{c_1}, \end{aligned} \quad (7)$$

where $\varepsilon_{c,v}$ are single-particle energies, W and V are the screened and bare Coulomb potentials. The numerical

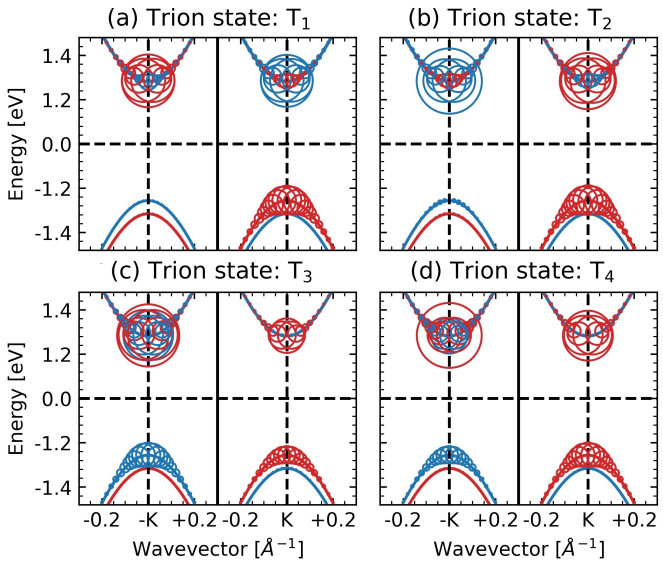

FIG. 3. Contributions of Dirac single-particle band states in the vicinity of the K and $-K$ points to trions (panels (a) - (d)). A circle position points to the single-particle state, and its radius gives weight to the exciton state; colors mark the spin projection s^z. The states T1 and T2 in panels (a) and (b) have $\tau s^z = 1/2$, and the states T3 and T4 in panels (c) and (d) have $\tau s^z = -1/2$. The results are shown for $E_F = 2.9$ meV. Adapted from[79].

implementation of the general Eq. (7) can be performed in the single particle basis set obtained from *ab initio* density functional theory[36], tight-binding model[54], or Dirac model Hamiltonian[40].

The influence of electron doping is taken into account by using the approach described in Ref.[54], where the Pauli blocking of the occupied electron states is modeled by choosing the discretized mesh with the interval δK in the Brillouin zone. The doping density $n = g_v g_s/(\Omega_0 N^2)$ is related to the number of mesh points $N \times N$ of the Brillouin zone and the area of the primitive cell Ω_0 (g_s and g_v are spin and valley degeneracies, respectively). The corresponding Fermi energy of the doping electrons is given by $E_F = \hbar^2 \delta k^2/2m$ where the discretization interval for the hexagonal lattice of the TMDC is $\delta k = 4\pi/(\sqrt{3}aN)$.

To find the trion wavefunctions and energies, the following eigenvalue problem must be solved:

$$\sum_{c_1' c_2' v'} H^{c_1' c_2' v'}_{c_1 c_2 v} A^T_{c_1' c_2' v'} = E_T A^T_{c_1 c_2 v}, \tag{8}$$

where E_T denotes the energy of the T-th trion, and $A^T_{c_1' c_2' v'}$ represents its wavefunction. In turn, the linear absorption spectrum for trions is determined by summing the transition rates between all possible free electron and three-particle states, resulting in the following expression:

$$L(\varepsilon) \propto \sum_{c,T} \left| \langle T|\hat{\mathbf{P}}|c\rangle \right|^2 \delta\left(\varepsilon - \varepsilon_T + \varepsilon_c\right), \tag{9}$$

where the summation is over single-electron states c and three-particle states T with the same momentum $\mathbf{k}$. Finally, the trion transition matrix element is calculated as:

$$\langle T|\hat{\mathbf{P}}|c\rangle = \sum_{c_1 c_2 v} A^T_{c_1 c_2 v} \left(\mathbf{p}_{c_1 v}\delta^{c_2}_c - \mathbf{p}_{c_2 v}\delta^{c_1}_c\right), \tag{10}$$

where $\mathbf{p}_{cv}$ represents the transition matrix element for conduction state c and valence state v.

III. TRION FINE STRUCTURE AND PHOTOLUMINESCENCE

In the case of photoluminescence, the emission occurs from the ensemble of thermally equilibrated excited states. Coulomb interaction lifts the degeneracy of the many-body excited states. One of the initial questions that arose from the experimental results[10,32] was the determination of the fine structure of the trion states. Several theoretical works have attempted to answer this question, such as the works[35,59], where a variational approach was used to determine the fine structure of trion states. The article[59] studied the interaction of light-matter and the non-equilibrium dynamics of exchange-split trions in a WS_2 monolayer using optical spectroscopy. The role of doping on trions and their fine structure has been explored by various experimental techniques in Ref.[44,108], including nonlinear spectroscopy[109–112]. The exact diagonalization approach of the three-particle problem was applied in work[41] and parameterized from the first principles in Ref.[39,50]. One of the earlier work [33] addressed the question of the dependence of the fine structure of the trion and exciton spectra on doping within the Fermi polaron approach to solving the trion problem. Subsequently, the approach of exact diagonalization of the three-particle problem also makes it possible to study the dependence of the trion and excitonic states on the doping level[40,54,90]. The paper[54] examines how doping a MoS_2 monolayer affects the properties of three-particle states and the optical activity of intervalley excitons, which are normally dark in undoped layers. Employing exact diagonalization within the Tamm-Dancoff approximation reveals that doping can brighten these excitons, suggesting new possibilities for tuning the optical characteristics of MoS_2 monolayers. The absorption spectrum of the MoS_2 monolayer from Ref.[54] is presented for different values of doping density in Fig. 1.

The study in Ref.[79] examines trion states in four TMDC monolayers: MoS_2, $MoSe_2$, WS_2, and WSe_2 using direct diagonalization of the three-body Hamiltonian, revealing that the fine structure results from the interaction

between the spin-valley fine structure of single-particle bands and particle-exchange interactions. Variations in doping and the dielectric environment can tune the trion energy fine structure, leading to the anti-crossing of bright and dark states, significantly affecting the optical spectra. The results of the calculations from Ref.[79] are presented in Fig. 2. This figure illustrates the optical transition energies of trions (indicated by circle positions) and their oscillator strengths (represented by circle size and color) as a function of electron doping (relative Fermi energy of the doping electrons). Two qualitatively different three-particle states were identified: "trions," where both electrons are tightly bound, and "excitons," where one electron is nearly free[40,54,90], making the state similar to a two-particle exciton weakly coupled to a single electron. The distinction between excitons and trions is evident in the doping dependence shown in Fig. 2. The energy of excitons increases with higher doping levels, while the energy of tightly bound trions shows a much weaker dependence on doping.

The spin-orbit coupling in $MoSe_2$, WS_2, and WSe_2, according to ab initio calculations[71,72,74], is significant and has the valley Zeeman form, leading to a conduction band splitting of approximately 20 meV. The Rashba coupling is minimal[71,72,74]. Thus, there is no spin-mixing effect, and spin can be considered a good quantum number in these systems. Unlike W-based materials, where the lowest energy state is typically dark, $MoSe_2$ has a bright lowest energy trion state due to its negative spin-orbit coupling splitting of the conduction band.

The internal structure of trion states, particularly the weights of the contributions from single-particle states, is crucial to understanding their optical properties. The single-particle contributions (single-particle density matrix) for the internal trions states T1-T4, calculated for a free-standing MoS_2 monolayer with a doping level of $E_F = 2.9$ meV, are illustrated in Fig. 3. This figure displays single-particle bands for electrons (positive energies) and holes (negative energies) near the K and -K valley points in the Brillouin zone. Blue and red colors indicate spin $s^z = \pm 1/2$ states. The center of each circle marks the energy contribution of the single-particle state, while the radius represents the weight of this state's contribution to the trion wave function. Due to strong intervalley mixing by the Coulomb interaction, a superposition of many single-particle states is created, making a simple representation of trions as a product of just a few states generally impossible.

The pair of trions T3 and T4 is a well-known singlet-triplet pair observed in earlier experimental and theoretical work[32,35,38,44,45,59,90,113–115]. In the T1 and T2 trion states, a hole is provided by a single valley ($-K$), while electrons from both valleys, having different spins, contribute. In the limit of vanishing doping, T1 is dark and T2 is bright due to the opposite spins of the valley electrons in these states. However, as doping increases, both the T1 and T2 states become bright. Conversely, the T3 and T4 states involve holes of opposite spins. At zero doping, T4 is an optically parity-favored state, while T1 is an optically spin-favored state. Additionally, the system has four equivalent trion states related to T1-T4 by symmetry transformation $K \leftrightarrow -K$.

Unlike the exciton, trion can not decay radiatively from the nonzero-momentum state, because the leftover electron helps to satisfy the momentum conservation law[40,46], which leads to unique characteristics in the photoluminescence spectra. In particular, the trion spectral

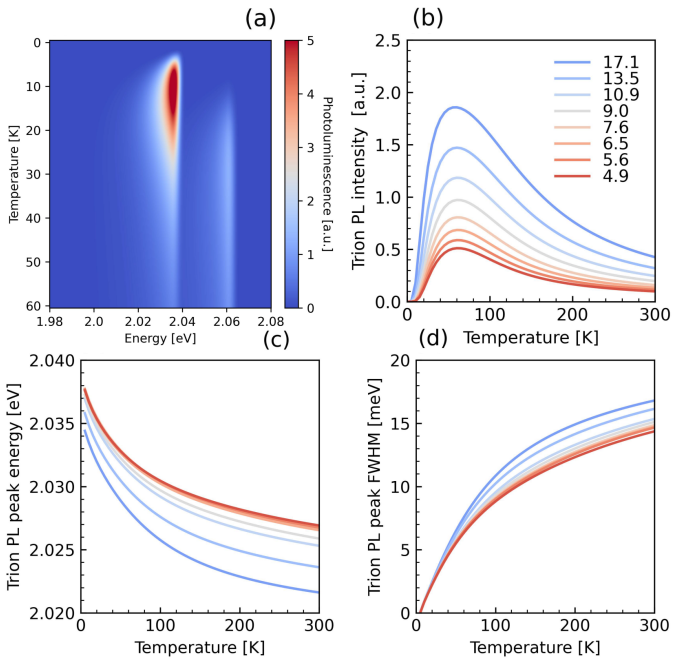

FIG. 4. (a) Photoluminescence spectra of a MoS_2 monolayer at $E_F = 4.9$ meV. Temperature dependence of the PL peak: (b) intensity of the trion peak, (c) energy position of the trion peak, and (d) width (full-width-half-maximum) of the trion peak, calculated for several values of the Fermi energy [shown in the legend (b) in meV's]. Adapted from[40].

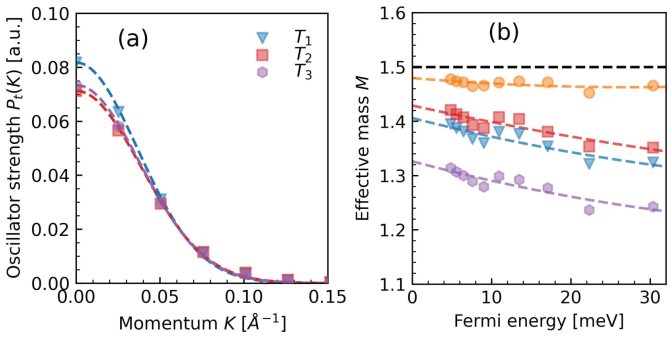

FIG. 5. (a) Momentum dependence of the trion oscillation strength of the three bright trion states. (b) Doping dependence trion effective mass M, The calculations are done for $E_F = 4.9$ meV. Adapted from[40].

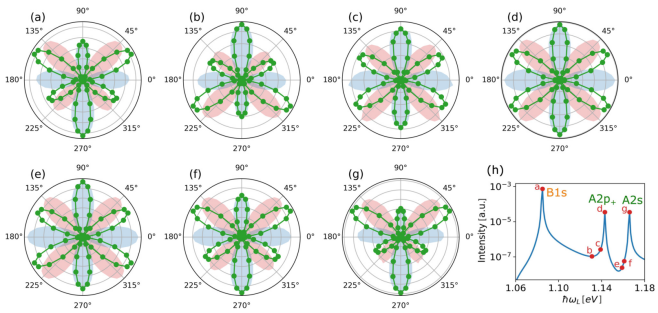

FIG. 6. Angular dependence of second harmonic generation intensity (green points) and polarization components $|P_x|^2$ (red shading) and $|P_y|^2$ (blue shading) calculated for driving field energies marked by the red points in (h). Adapted from[116,117].

peak broadens and redshifts with temperature, even in the absence of electron-phonon interaction. Fig. 4 shows photoluminescence spectra of MoS_2 monolayer, following Ref.[40]. Calculations reveal that the trion peak characteristics, such as transition energy, intensity, shape, and width, are highly sensitive to changes in temperature and doping levels.

At low temperatures, the exciton peak is almost absent and becomes visible only when the temperature exceeds 70 K, increasing in intensity as the temperature rises. In contrast, the trion peak appears at temperatures as low as 10 K and demonstrates a sharp non-monotonic temperature dependence, peaking at around 65 K before rapidly declining. With increased doping, the trion peak shifts to lower energies, resulting in a redshift, while the exciton peak splits and moves to higher energies. The intensity of the trion peak increases with higher doping levels, and the peak becomes asymmetrically broader at elevated temperatures, with the left wing of the peak significantly wider than the right.

The transition dipole for trion, shown in Fig. 5a, reveals the momentum dependence of all optically bright branches of the trion states. The radiative decay of trions is allowed up to a finite momentum cutoff determined by the inverse of the effective radius of the trion[40]. The effective mass of the trion M, shown in Fig. 5b, is renormalized from the noninteracting value of $2m_c + m_v$ by Coulomb interactions, where m_c and m_v are the masses of the conduction and valence bands. This effect is caused by the fill factor effect, and the dielectric constant change caused by doping is not included in the calculations in Fig. 5b.

IV. NON-LINEAR OPTICAL EFFECTS

SHG measurements are shown to be particularly effective in probing electronic excitations, allowing researchers to study the band structure and interband transitions in detail. This method fills the gap left by traditional linear spectroscopy techniques such as Raman and photoluminescence spectroscopy. Unlike linear response spectra, SHG signals require a more complex theoretical analysis. This analysis involves solving the complete non-linear dynamical problem, which is essential for understanding the behavior of materials under strong excitations and highly nonlinear dynamics. Strong linear absorption in TMDCs implies a strong non-linear response, and the many-body effects need to be included explicitly. In Ref.[118], the non-linear response was calculated within the GW-BSE approach. Excitonic effects were shown to be very strong in non-linear second-order response calculations[119] in another example of low-dimensional material, carbon nanotubes.

One of the notable findings of the paper[116,117] is the role of excitons in altering the SHG polarization angular dependence, as shown in Fig. 6. The SHG signal increases significantly when the driving pulse resonates with an excitonic state. Excitons also induce qualitative changes in the SHG polarization angular dependence, which varies with the energy and amplitude of the driving field depending on the type of resonating exciton. These changes result in deviations from the symmetric six-leaf angular dependence observed in TMDCs monolayers with an undistorted crystal structure

V. EXCITON DYNAMICS UNDER EXTERNAL PERTURBATIONS

One of the clear examples of the interaction of exciton states under external interactions is the formation exciton-polaritons quasiparticles, which are formed from the strong coupling between excitons and photons in semiconductor microcavities[121–123] as well as photons and trions[124,125], which can be probed by both linear and nonlinear spectroscopy[126–129]. The simulation study shows the absorption spectra of MoS_2 monolayer in Fig. 7, which results from the interaction between material optical excitations and a cavity mode. It provides a comprehensive microscopic theory for exciton-polariton states across different doping levels by solving the three-body problem through exact diagonalization of the Hamiltonian (8). Various polaritonic modes were predicted, including exciton-polaritons and trion-polaritons, some of them become bright due to interactions between excitons and free carriers. Highlighting the importance of strong light-matter coupling, the research shows how increased doping modifies the optical response of TMDC monolayers due to bandgap renormalization, screening effects, and Pauli blocking, leading to the formation of trions and exciton polarons. This results in significant changes in the absorption spectrum, with additional bright polaritonic modes appearing at higher doping levels, as demonstrated in Fig. 7. Similarly, cavity-induced splitting of dark-bright excitons into two hybrid exciton–polariton states reversing the energy

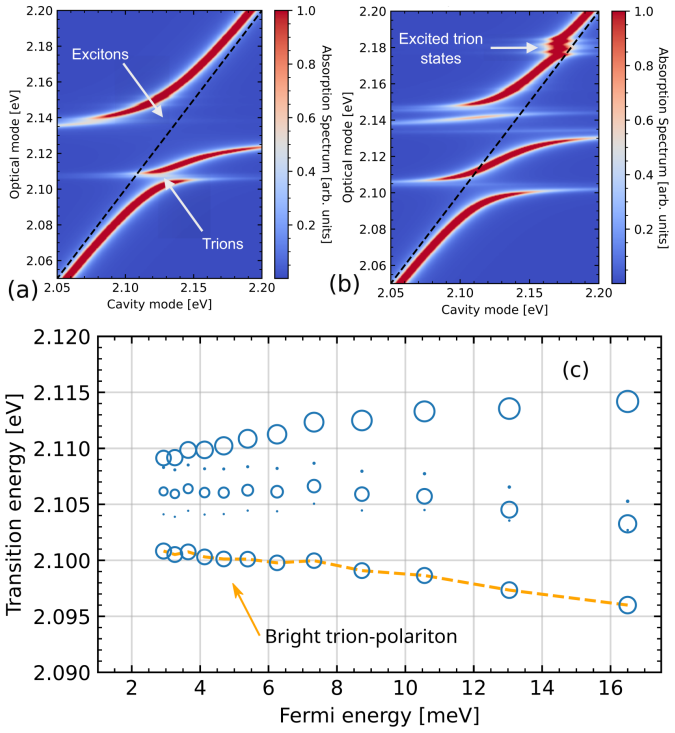

FIG. 7. Absorption spectra in MoS_2 monalayer placed in the cavity as a function of the cavity resonance detuning for low and high doping levels: (a) $E_F = 3.26$ meV and (b) $E_F = 21.55$ meV. (c) Doping dependence of trion polaritons in MoS_2 monolayer, where cavity mode is tuned close in energy to the trion modes. The cavity-modified ground state is bright, thus enabling efficient photoluminescence from the system. The cavity mode is at $E_0 = 2.14$ eV. Adapted from[120].

order of the dark and bright states has recently been predicted in carbon nanotubes[130].

Another example of external perturbation involves the application of an in-plane electric field to TMDC. The excitonic Stark effect refers to changes in the energy levels and optical properties of excitons in response to an external electric field. The Stark effect for free excitons in MoS_2 was predicted in Ref.[131] and was subsequently measured in Ref.[132]. The interplay between the electric field and the interactions between excitons and the surrounding environment strongly influenced the excitonic Stark effect and the field ionization of bound excitons in monolayers[131].

VI. OUTLOOK

In this Perspective, we provide a comprehensive overview of the current state of knowledge of trions and excitons in transition-metal dichalcogenides. We highlight the potential of monolayers as optoelectronic materials and the importance of understanding the impact of external factors, such as temperature, doping concentration, external in-plane electric field, cavity mode electric field, and the dielectric environment, on their optical properties. The analysis of three-particle states in TMDC monolayers, based on a direct diagonalization of the corresponding Hamiltonian, classifies the fine structure of the low-energy trion and exciton states and spectral properties of doped TMDCs.

Theoretical models, particularly those incorporating many-body interactions, have demonstrated a valuable insight into the nature of optical spectra in monolayer TMDCs. In particular predicted exciton and trion binding energies, optical band gaps, and absorption spectra agree well with the available experimental results. However, discrepancies still exist in fine-structure energy details due to the uncertainties in environmental effects, such as dielectric screening, defects, accidental strain and doping in real samples. These mismatches can also stem from simplifications in theoretical models, such restrictions to two- and three- body problems and the limitations of current computational power in solving higher-order many-body effects. To address these gaps, improvements are needed in refining calculations to include of real-world factors like defects and strain. Emphasizing such areas will not only enhance the predictive power of theoretical models but also strengthen their alignment with experimental findings, driving further advancements in the field.

While this Perspective primarily focuses on the results for monolayer TMDCs, there is significant interest in van der Waals heterostructures[133] (and references therein). Similar theoretical frameworks should be applied to investigate the optical properties of heterobilayers, which present additional degrees of freedom. For instance, the interlayer distance largely dictates the interlayer exciton radius and, consequently, the binding energy. While first-principles calculations have provided valuable insights into band alignment in heterobilayers and the corresponding effective masses, ongoing research actively explores many-body solutions for such complex systems. The Perspective overviews explanations of existing experimental observations of trion states in 2D multivalley materials and provides new insights into the external perturbations on linear and nonlinear optical spectra in TMDCs monolayers.

ACKNOWLEDGMENTS

We gratefully acknowledge the support by the National Science Foundation under Grant No. 2235276.

AUTHOR DECLARATIONS

CONFLICT OF INTEREST

The authors have no conflicts to disclose.

DATA AVAILABILITY

Data sharing is not applicable to this article as no new data were created or analyzed in this study.

* Authors to whom correspondence should be addressed: Y.V.Z. - iaroslav.zhumagulov@ur.de, V.P. - vasilipe@buffalo.edu

[1] K. F. Mak, C. Lee, J. Hone, J. Shan, and T. F. Heinz, Phys. Rev. Lett. **105**, 136805 (2010).
[2] A. Splendiani, L. Sun, Y. Zhang, T. Li, J. Kim, C.-Y. Chim, G. Galli, and F. Wang, Nano Lett. **10**, 1271 (2010).
[3] H.-P. Komsa and A. V. Krasheninnikov, Phys. Rev. B **86**, 241201 (2012).
[4] J. Feng, X. Qian, C.-W. Huang, and J. Li, Nat. Photonics **6**, 866 (2012).
[5] D. Y. Qiu, F. H. da Jornada, and S. G. Louie, Phys. Rev. Lett. **111**, 216805 (2013).
[6] I. B. Amara, E. B. Salem, and S. Jaziri, J. Appl. Phys. **120**, 051707 (2016).
[7] J. F. Muth, J. H. Lee, I. K. Shmagin, R. M. Kolbas, H. C. Casey, B. P. Keller, U. K. Mishra, and S. P. DenBaars, Applied Physics Letters **71**, 2572 (1997).
[8] P. Y. Yu and M. Cardona, *Fundamentals of Semiconductors* (Springer Berlin Heidelberg, 2010).
[9] M. Dvorak, S.-H. Wei, and Z. Wu, Physical Review Letters **110**, 016402 (2013).
[10] K. F. Mak, K. He, C. Lee, G. H. Lee, J. Hone, T. F. Heinz, and J. Shan, Nat. Mater. **12**, 207 (2012).
[11] S. Mouri, Y. Miyauchi, and K. Matsuda, Nano Lett. **13**, 5944 (2013).
[12] J. S. Ross, P. Klement, A. M. Jones, N. J. Ghimire, J. Yan, D. G. Mandrus, T. Taniguchi, K. Watanabe, K. Kitamura, W. Yao, D. H. Cobden, and X. Xu, Nat. Nanotechnol. **9**, 268 (2014).
[13] C. Lui, A. Frenzel, D. Pilon, Y.-H. Lee, X. Ling, G. Akselrod, J. Kong, and N. Gedik, Phys. Rev. Lett. **113**, 166801 (2014).
[14] C. Zhang, H. Wang, W. Chan, C. Manolatou, and F. Rana, Phys. Rev. B **89**, 205436 (2014).
[15] N. Scheuschner, O. Ochedowski, A.-M. Kaulitz, R. Gillen, M. Schleberger, and J. Maultzsch, Phys. Rev. B **89**, 125406 (2014).
[16] R. Soklaski, Y. Liang, and L. Yang, Appl. Phys. Lett. **104**, 193110 (2014).
[17] Y. Zhang, H. Li, H. Wang, R. Liu, S.-L. Zhang, and Z.-J. Qiu, ACS Nano **9**, 8514 (2015).
[18] A. R. Rezk, B. Carey, A. F. Chrimes, D. W. M. Lau, B. C. Gibson, C. Zheng, M. S. Fuhrer, L. Y. Yeo, and K. Kalantar-zadeh, Nano Lett. **16**, 849 (2016).
[19] A. Singh, G. Moody, K. Tran, M. E. Scott, V. Overbeck, G. Berghäuser, J. Schaibley, E. J. Seifert, D. Pleskot, N. M. Gabor, J. Yan, D. G. Mandrus, M. Richter, E. Malic, X. Xu, and X. Li, Phys. Rev. B **93**, 041401 (2016).
[20] Y. You, X.-X. Zhang, T. C. Berkelbach, M. S. Hybertsen, D. R. Reichman, and T. F. Heinz, Nature Physics **11**, 477 (2015).
[21] E. J. Sie, A. J. Frenzel, Y.-H. Lee, J. Kong, and N. Gedik, Physical Review B **92**, 125417 (2015).
[22] G. Plechinger, P. Nagler, J. Kraus, N. Paradiso, C. Strunk, C. Schüller, and T. Korn, Physica Status Solidi **9**, 457 (2015).
[23] K. Hao, J. F. Specht, P. Nagler, L. Xu, K. Tran, A. Singh, C. K. Dass, C. Schüller, T. Korn, M. Richter, A. Knorr, X. Li, and G. Moody, Nature Communications **8**, 15552 (2017).
[24] I. Paradisanos, S. Germanis, N. T. Pelekanos, C. Fotakis, E. Kymakis, G. Kioseoglou, and E. Stratakis, Applied Physics Letters **110**, 193102 (2017).
[25] Z. Ye, L. Waldecker, E. Y. Ma, D. Rhodes, A. Antony, B. Kim, X.-X. Zhang, M. Deng, Y. Jiang, Z. Lu, D. Smirnov, K. Watanabe, T. Taniguchi, J. Hone, and T. F. Heinz, Nature Communications **9**, 3718 (2018).
[26] A. Torche and G. Bester, Communications Physics **4**, 67 (2021).
[27] M. Gmitra and J. Fabian, Physical Review Letters **119**, 146401 (2017).
[28] C. J. Ciccarino, T. Christensen, R. Sundararaman, and P. Narang, Nano Letters **18**, 5709 (2018).
[29] L. L. Tao and E. Y. Tsymbal, Physical Review B **100**, 161110(R) (2019).
[30] Y. Wang, L. Deng, Q. Wei, Y. Wan, Z. Liu, X. Lu, Y. Li, L. Bi, L. Zhang, H. Lu, H. Chen, P. Zhou, L. Zhang, Y. Cheng, X. Zhao, Y. Ye, W. Huang, S. J. Pennycook, K. P. Loh, and B. Peng, Nano Letters **20**, 2129 (2020).
[31] B. Ganchev, N. Drummond, I. Aleiner, and V. Fal'ko, Physical Review Letters **114**, 107401 (2015).
[32] G. Plechinger, P. Nagler, A. Arora, R. Schmidt, A. Chernikov, A. G. del Águila, P. C. Christianen, R. Bratschitsch, C. Schüller, and T. Korn, Nature Communications **7**, 12715 (2016).
[33] D. K. Efimkin and A. H. MacDonald, Phys. Rev. B **95**, 035417 (2017).
[34] E. Mostaani, M. Szyniszewski, C. H. Price, R. Maezono, M. Danovich, R. J. Hunt, N. D. Drummond, and V. I. Fal'ko, Physical Review B **96**, 075431 (2017).
[35] E. Courtade, M. Semina, M. Manca, M. M. Glazov, C. Robert, F. Cadiz, G. Wang, T. Taniguchi, K. Watanabe, M. Pierre, W. Escoffier, E. L. Ivchenko, P. Renucci, X. Marie, T. Amand, and B. Urbaszek, Phys. Rev. B **96**, 085302 (2017).
[36] M. Drüppel, T. Deilmann, P. Krüger, and M. Rohlfing, Nat. Commun. **8**, 2117 (2017).
[37] G. Wang, A. Chernikov, M. M. Glazov, T. F. Heinz, X. Marie, T. Amand, and B. Urbaszek, Rev. Mod. Phys. **90**, 021001 (2018).
[38] A. Arora, N. K. Wessling, T. Deilmann, T. Reichenauer, P. Steeger, P. Kossacki, M. Potemski, S. Michaelis de Vasconcellos, M. Rohlfing, and R. Bratschitsch, Phys. Rev. B(R) **101**, 241413 (2020).
[39] A. Torche and G. Bester, Phys. Rev. B **100**, 201403 (2019).
[40] Y. V. Zhumagulov, A. Vagov, D. R. Gulevich, P. E. F. Junior, and V. Perebeinos, The Journal of Chemical Physics

153, 044132 (2020).
[41] A. Hichri and S. Jaziri, Physical Review B **102**, 085407 (2020).
[42] M. Grzeszczyk, K. Olkowska-Pucko, K. Nogajewski, K. Watanabe, T. Taniguchi, P. Kossacki, A. Babiński, and M. R. Molas, Nanoscale **13**, 18726 (2021).
[43] J. Jadczak, J. Kutrowska-Girzycka, M. Bieniek, T. Kazimierczuk, P. Kossacki, J. J. Schindler, J. Debus, K. Watanabe, T. Taniguchi, C. H. Ho, A. Wójs, P. Hawrylak, and L. Bryja, Nanotechnology **32**, 145717 (2021).
[44] M. Zinkiewicz, T. Woźniak, T. Kazimierczuk, P. Kapuscinski, K. Oreszczuk, M. Grzeszczyk, M. Bartoš, K. Nogajewski, K. Watanabe, T. Taniguchi, C. Faugeras, P. Kossacki, M. Potemski, A. Babiński, and M. R. Molas, Nano Letters **21**, 2519 (2021).
[45] Y.-W. Chang and Y.-C. Chang, The Journal of Chemical Physics **155**, 024110 (2021).
[46] J. W. Christopher, B. B. Goldberg, and A. K. Swan, Scientific Reports **7**, 14062 (2017).
[47] D. W. Hamby, D. A. Lucca, M. J. Klopfstein, and G. Cantwell, Journal of Applied Physics **93**, 3214 (2003).
[48] A. R. Amori, J. E. Rossi, B. J. Landi, and T. D. Krauss, The Journal of Physical Chemistry C **122**, 3599 (2018).
[49] S. Golovynskyi, M. Bosi, L. Seravalli, and B. Li, Surfaces and Interfaces **23**, 100909 (2021).
[50] T. Deilmann and K. S. Thygesen, Phys. Rev. B **96**, 201113 (2017).
[51] P. Li, C. Robert, D. Van Tuan, L. Ren, M. Yang, X. Marie, and H. Dery, Phys. Rev. B **106**, 085414 (2022).
[52] S. B. Chand, J. M. Woods, J. Quan, E. Mejia, T. Taniguchi, K. Watanabe, A. Alù, and G. Grosso, Nature Communications **14**, 3712 (2023).
[53] B. Scharf and V. Perebeinos, The Journal of Chemical Physics **161**, 134709 (2024).
[54] Y. V. Zhumagulov, A. Vagov, N. Y. Senkevich, D. R. Gulevich, and V. Perebeinos, Phys. Rev. B **101**, 245433 (2020).
[55] T. C. Berkelbach, M. S. Hybertsen, and D. R. Reichman, Phys. Rev. B **88**, 045318 (2013).
[56] K.-Q. Lin, J. D. Ziegler, M. A. Semina, J. V. Mamedov, K. Watanabe, T. Taniguchi, S. Bange, A. Chernikov, M. M. Glazov, and J. M. Lupton, Nature Communications **13** (2022), 10.1038/s41467-022-33939-w.
[57] M. V. Durnev and M. M. Glazov, Physics-Uspekhi **61**, 825–845 (2018).
[58] M. A. Semina, J. V. Mamedov, and M. M. Glazov, Oxford Open Materials Science **3**, itad004 (2023).
[59] J. Zipfel, K. Wagner, J. D. Ziegler, T. Taniguchi, K. Watanabe, M. A. Semina, and A. Chernikov, The Journal of Chemical Physics **153**, 034706 (2020).
[60] S. Albrecht, L. Reining, R. Del Sole, and G. Onida, Phys. Rev. Lett. **80**, 4510 (1998).
[61] L. X. Benedict, E. L. Shirley, and R. B. Bohn, Phys. Rev. Lett. **80**, 4514 (1998).
[62] M. Rohlfing and S. G. Louie, Phys. Rev. Lett. **80**, 3320 (1998).
[63] M. Rohlfing and S. G. Louie, Phys. Rev. Lett. **81**, 2312 (1998).
[64] M. Rohlfing and S. G. Louie, Phys. Rev. Lett. **82**, 1959 (1999).
[65] M. Rohlfing and S. G. Louie, Phys. Rev. Lett. **83**, 856 (1999).
[66] M. Rohlfing and S. G. Louie, Phys. Rev. B **62**, 4927 (2000).
[67] N. S. Rytova, Moscow University Physics Bulletin **3**, 18 (1967).
[68] L. V. Keldysh, Soviet Journal of Experimental and Theoretical Physics Letters **29**, 658 (1979).
[69] P. Cudazzo, I. V. Tokatly, and A. Rubio, Phys. Rev. B **84**, 085406 (2011).
[70] M. Florian, M. Hartmann, A. Steinhoff, J. Klein, A. W. Holleitner, J. J. Finley, T. O. Wehling, M. Kaniber, and C. Gies, Nano Letters **18**, 2725 (2018).
[71] D. Xiao, G.-B. Liu, W. Feng, X. Xu, and W. Yao, Phys. Rev. Lett. **108**, 196802 (2012).
[72] A. Kormányos, G. Burkard, M. Gmitra, J. Fabian, V. Zólyomi, N. D. Drummond, and V. Fal'ko, 2D Mater. **2**, 022001 (2015).
[73] C. Zhang, C. Gong, Y. Nie, K.-A. Min, C. Liang, Y. J. Oh, H. Zhang, W. Wang, S. Hong, L. Colombo, R. M. Wallace, and K. Cho, 2D Materials **4**, 015026 (2016).
[74] K. Zollner, P. E. F. Junior, and J. Fabian, Phys. Rev. B **100**, 195126 (2019).
[75] Y. Cho and T. C. Berkelbach, Phys. Rev. B **97**, 041409(R) (2018).
[76] L. Waldecker, A. Raja, M. Rösner, C. Steinke, A. Bostwick, R. J. Koch, C. Jozwiak, T. Taniguchi, K. Watanabe, E. Rotenberg, T. O. Wehling, and T. F. Heinz, Physical Review Letters **123**, 206403 (2019).
[77] A. Raja, A. Chaves, J. Yu, G. Arefe, H. M. Hill, A. F. Rigosi, T. C. Berkelbach, P. Nagler, C. Schüller, T. Korn, C. Nuckolls, J. Hone, L. E. Brus, T. F. Heinz, D. R. Reichman, and A. Chernikov, Nature Communications **8**, 15251 (2017).
[78] A. Laturia, M. L. V. de Put, and W. G. Vandenberghe, npj 2D Materials and Applications **2**, 6 (2018).
[79] Y. V. Zhumagulov, A. Vagov, D. R. Gulevich, and V. Perebeinos, Nanomaterials **12** (2022), 10.3390/nano12213728.
[80] T. Deilmann, M. Drüppel, and M. Rohlfing, Phys. Rev. Lett. **116**, 196804 (2016).
[81] T. Deilmann and K. S. Thygesen, Nano Letters **18**, 1460–1465 (2018).
[82] A. Arora, T. Deilmann, T. Reichenauer, J. Kern, S. Michaelis de Vasconcellos, M. Rohlfing, and R. Bratschitsch, Phys. Rev. Lett. **123**, 167401 (2019).
[83] T. Deilmann and K. S. Thygesen, 2D Mater. **5**, 041007 (2018).
[84] T. Deilmann and M. Rohlfing, Nano Lett. **17**, 6833 (2017).
[85] T. Deilmann, Phys. Rev. B **98**, 165105 (2018).
[86] M. R. Carbone, M. Z. Mayers, and D. R. Reichman, The Journal of Chemical Physics **152** (2020), 10.1063/5.0008730.
[87] L. S. R. Cavalcante, D. R. da Costa, G. A. Farias, D. R. Reichman, and A. Chaves, Phys. Rev. B **98**, 245309 (2018).
[88] Y.-W. Chang and D. R. Reichman, Phys. Rev. B **99**, 125421 (2019).
[89] Y. Cho, S. M. Greene, and T. C. Berkelbach, Phys. Rev. Lett. **126**, 216402 (2021).
[90] R. Tempelaar and T. C. Berkelbach, Nature Communications **10** (2019), 10.1038/s41467-019-11497-y.
[91] R. Y. Kezerashvili and S. M. Tsiklauri, Few-Body Syst. **58**, 18 (2016).
[92] J. R. Engelbrecht and M. Randeria, Phys. Rev. Lett. **65**, 1032 (1990).
[93] J. R. Engelbrecht and M. Randeria, Phys. Rev. B **45**, 12419 (1992).

[94] R. Schmidt and T. Enss, Phys. Rev. A **83**, 063620 (2011).
[95] R. Schmidt, T. Enss, V. Pietilä, and E. Demler, Phys. Rev. A **85**, 021602 (2012).
[96] Z. A. Iakovlev and M. M. Glazov, 2D Materials **10**, 035034 (2023).
[97] M. Sidler, P. Back, O. Cotlet, A. Srivastava, T. Fink, M. Kroner, E. Demler, and A. Imamoglu, Nature Physics **13**, 255–261 (2016).
[98] A. Tiene, B. C. Mulkerin, J. Levinsen, M. M. Parish, and F. M. Marchetti, Phys. Rev. B **108**, 125406 (2023).
[99] D. Huang, K. Sampson, Y. Ni, Z. Liu, D. Liang, K. Watanabe, T. Taniguchi, H. Li, E. Martin, J. Levinsen, M. M. Parish, E. Tutuc, D. K. Efimkin, and X. Li, Phys. Rev. X **13**, 011029 (2023).
[100] J. B. Muir, J. Levinsen, S. K. Earl, M. A. Conway, J. H. Cole, M. Wurdack, R. Mishra, D. J. Ing, E. Estrecho, Y. Lu, D. K. Efimkin, J. O. Tollerud, E. A. Ostrovskaya, M. M. Parish, and J. A. Davis, Nature Communications **13** (2022), 10.1038/s41467-022-33811-x.
[101] D. K. Efimkin and A. H. MacDonald, Phys. Rev. B **97**, 235432 (2018).
[102] E. Laird, F. M. Marchetti, D. K. Efimkin, M. M. Parish, and J. Levinsen, Phys. Rev. B **106**, 125407 (2022).
[103] I. Amelio, N. D. Drummond, E. Demler, R. Schmidt, and A. Imamoglu, Phys. Rev. B **107**, 155303 (2023).
[104] C. Fey, P. Schmelcher, A. Imamoglu, and R. Schmidt, Phys. Rev. B **101**, 195417 (2020).
[105] D. K. Efimkin, E. K. Laird, J. Levinsen, M. M. Parish, and A. H. MacDonald, Phys. Rev. B **103**, 075417 (2021).
[106] M. M. Glazov, The Journal of Chemical Physics **153**, 034703 (2020).
[107] R. Suris, V. Kochereshko, G. Astakhov, D. Yakovlev, W. Ossau, J. Nürnberger, W. Faschinger, G. Landwehr, T. Wojtowicz, G. Karczewski, and J. Kossut, physica status solidi (b) **227**, 343 (2001).
[108] Z. Li, T. Wang, Z. Lu, M. Khatoniar, Z. Lian, Y. Meng, M. Blei, T. Taniguchi, K. Watanabe, S. A. McGill, S. Tongay, V. M. Menon, D. Smirnov, and S.-F. Shi, Nano Letters **19**, 6886 (2019).
[109] A. Singh, G. Moody, S. Wu, Y. Wu, N. J. Ghimire, J. Yan, D. G. Mandrus, X. Xu, and X. Li, Phys. Rev. Lett. **112**, 216804 (2014).
[110] G. Wang, X. Marie, I. Gerber, T. Amand, D. Lagarde, L. Bouet, M. Vidal, A. Balocchi, and B. Urbaszek, Phys. Rev. Lett. **114**, 097403 (2015).
[111] K. L. Seyler, J. R. Schaibley, P. Gong, P. Rivera, A. M. Jones, S. Wu, J. Yan, D. G. Mandrus, W. Yao, and X. Xu, Nature Nanotechnology **10**, 407 (2015).
[112] C. T. Le, D. J. Clark, F. Ullah, J. I. Jang, V. Senthilkumar, Y. Sim, M.-J. Seong, K.-H. Chung, J. W. Kim, S. Park, S. H. Rhim, G. Kim, and Y. S. Kim, ACS Photonics **4**, 38 (2017).
[113] D. Vaclavkova, J. Wyzula, K. Nogajewski, M. Bartos, A. O. Slobodeniuk, C. Faugeras, M. Potemski, and M. R. Molas, Nanotechnology **29**, 325705 (2018).
[114] G. Plechinger, P. Nagler, A. Arora, A. G. del Águila, M. V. Ballottin, T. Frank, P. Steinleitner, M. Gmitra, J. Fabian, P. C. M. Christianen, R. Bratschitsch, C. Schüller, and T. Korn, Nano Letters **16**, 7899 (2016).
[115] J. Fu, J. M. R. Cruz, and F. Qu, Applied Physics Letters **115**, 082101 (2019).
[116] Y. V. Zhumagulov, V. D. Neverov, A. E. Lukyanov, D. R. Gulevich, A. V. Krasavin, A. Vagov, and V. Perebeinos, Phys. Rev. B **105**, 115436 (2022).
[117] Y. V. Zhumagulov, V. D. Neverov, A. E. Lukyanov, D. R. Gulevich, A. V. Krasavin, A. Vagov, and V. Perebeinos, Phys. Rev. B **105**, 239902 (2022).
[118] V. Chang Lee, L. Yue, M. B. Gaarde, Y.-h. Chan, and D. Y. Qiu, Nature Communications **15**, 6228 (2024).
[119] J. Rui Xu, V. Doumani, N. Labuntsov, A.-C. Hong, W. Samaha, F. Tu, E. Tay, J. Blackert, M. E. Luo, W. Tahchi, J. Gao, Y. Lou, K. Yomogida, R. Yanagi, V. Saito, A. Perebeinos, J. Baydin, H. Kono, and Zhu, arXiv:2407.04514 (2024).
[120] Y. V. Zhumagulov, S. Chiavazzo, D. R. Gulevich, V. Perebeinos, I. A. Shelykh, and O. Kyriienko, npj Computational Materials **8**, 92 (2022).
[121] A. V. Kavokin, J. J. Baumberg, G. Malpuech, and F. P. Laussy, *Microcavities* (Oxford University Press, Oxford, 2007).
[122] H. M. Gibbs, G. Khitrova, and S. W. Koch, Nature Photonics **5**, 273 (2011).
[123] S. Dufferwiel, S. Schwarz, F. Withers, A. A. P. Trichet, F. Li, M. Sich, O. Del Pozo-Zamudio, C. Clark, A. Nalitov, D. D. Solnyshkov, G. Malpuech, K. S. Novoselov, J. M. Smith, M. S. Skolnick, D. N. Krizhanovskii, and A. I. Tartakovskii, Nature Communications **6**, 8579 (2015).
[124] S. Dhara, C. Chakraborty, K. M. Goodfellow, L. Qiu, T. A. O'Loughlin, G. W. Wicks, S. Bhattacharjee, and A. N. Vamivakas, Nature Physics **14**, 130 (2018).
[125] Y. Koo, H. Lee, T. Ivanova, A. Kefayati, V. Perebeinos, E. Khestanova, V. Kravtsov, and K.-D. Park, Light: Science & Applications **12**, 59 (2023).
[126] J. K. Day, M.-H. Chung, Y.-H. Lee, and V. M. Menon, Opt. Mater. Express **6**, 2360 (2016).
[127] M. Kilinc, A. Cheney, C. Neureuter, S. Tarasek, G. Xu, and T. Thomay, Opt. Mater. Express **11**, 1603 (2021).
[128] Z. Lin, X. Liang, M. Lončar, S. G. Johnson, and A. W. Rodriguez, Optica **3**, 233 (2016).
[129] S. Busschaert, R. Reimann, M. Cavigelli, R. Khelifa, A. Jain, and L. Novotny, ACS Photonics **7**, 2482 (2020).
[130] V. A. Shahnazaryan, V. A. Saroka, I. A. Shelykh, W. L. Barnes, and M. E. Portnoi, ACS Photonics **6**, 904 (2019).
[131] B. Scharf, T. Frank, M. Gmitra, J. Fabian, I. Žutić, and V. Perebeinos, Phys. Rev. B **94**, 245434 (2016).
[132] J. G. Roch, N. Leisgang, G. Froehlicher, P. Makk, K. Watanabe, T. Taniguchi, C. Schönenberger, and R. J. Warburton, Nano Letters **18**, 1070 (2018).
[133] A. Ciarrocchi, F. Tagarelli, A. Avsar, and A. Kis, Nature Reviews Materials **7**, 449 (2022).